

# CASL Structural Mechanics Modeling of Grid-to-Rod Fretting (GTRF)

WEI LU,<sup>1,4</sup> M.D. THOULESS,<sup>1,2</sup> ZUPAN HU,<sup>1</sup> HAI WANG,<sup>1</sup>  
RAMIN GHELICHI,<sup>3</sup> CHEN-HUNG WU,<sup>3</sup> KEN KAMRIN,<sup>3</sup>  
and DAVID PARKS<sup>3</sup>

1.—Department of Mechanical Engineering, University of Michigan, Ann Arbor, MI 48109, USA. 2.—Department of Materials Science and Engineering, University of Michigan, Ann Arbor, MI 48109, USA. 3.—Department of Mechanical Engineering, Massachusetts Institute of Technology, Cambridge, MA 02139, USA. 4.—e-mail: weilu@umich.edu

Fluid-induced grid-to-rod fretting (GTRF) wear is responsible for over 70% of fuel leaks in pressurized water reactors (PWRs) in the US. The Consortium for Advanced Simulation of Light Water Reactors (CASL) has identified GTRF as a challenge problem that is very important to nuclear plants. GTRF is a complex problem that involves multiple physical phenomena. This paper summarizes several GTRF-related problems being addressed by the University of Michigan and the Massachusetts Institute of Technology, CASL partners. These include analyses of cladding creep, wear, structural mechanics, and the effects of the rod-to-grid gap. Also outlined are additional aspects of material science and computational modeling that will be needed to realize the ultimate goal of high-fidelity predictive modeling and design tools to address GTRF.

## INTRODUCTION

Grid-to-rod fretting (GTRF) wear is responsible for over 70% of the fuel leaks in pressurized-water reactors (PWRs) in the US.<sup>1</sup> One of the main causes of failure has been identified as the relaxation of the grid-to-rod support in the assembly and flow-induced vibration.

The occurrence and progression of GTRF is closely related to the structure of the fuel assembly. In a fuel assembly, the fuel rods are supported by the springs and dimples of the spacer grid (Fig. 1). The initial preload between the grid and the fuel rod can prevent gross sliding between the two components in response to the turbulent flow of the coolant. However, this flow can cause partial slip at the edges of each contact, resulting in local fretting wear. Furthermore, the initial preload will relax over time because of deformation processes that take place as the reactor operates. As a result of this, the contact force between the grid and the fuel rod can relax to such an extent that gross sliding occurs between them, which enhances the fretting wear. The wear scar that forms during this process further accelerates the relaxation of the

contact force. Eventually, the grid can no longer maintain continuous contact with the fuel rod, and a gap will open up between them. This gap can induce larger amplitudes of vibration and dynamic impact between the contacts, and some have suggested this may result in a significant increase in the wear.<sup>2,3</sup>

Reliable simulations of GTRF require integration of quasi-static (in the early stage of wear) and dynamic (after a gap opens) structural analyses, turbulent-flow calculations, the modeling of material behavior at high temperatures and in an irradiation environment, and the simulation of local contact and wear. Here, we review recent advances in modeling techniques for GTRF-related problems, with a summary of some results of completed and in-progress research related to creep, wear, turbulent flow, structural analysis and the coupling of wear and creep.

## CREEP

To model creep correctly one needs to be able to capture the changes in the dominant mechanism that occur with changes in both temperature and

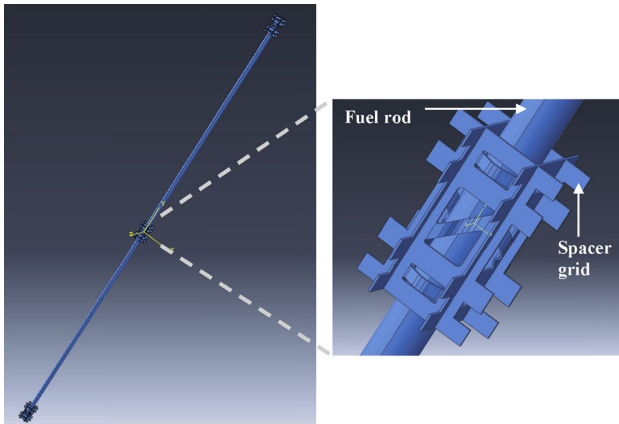


Fig. 1. A cell of the fuel assembly showing a fuel rod and the spacer grid. This model is based on a standard design for the  $17 \times 17$  Vantage5H fuel.<sup>4</sup>

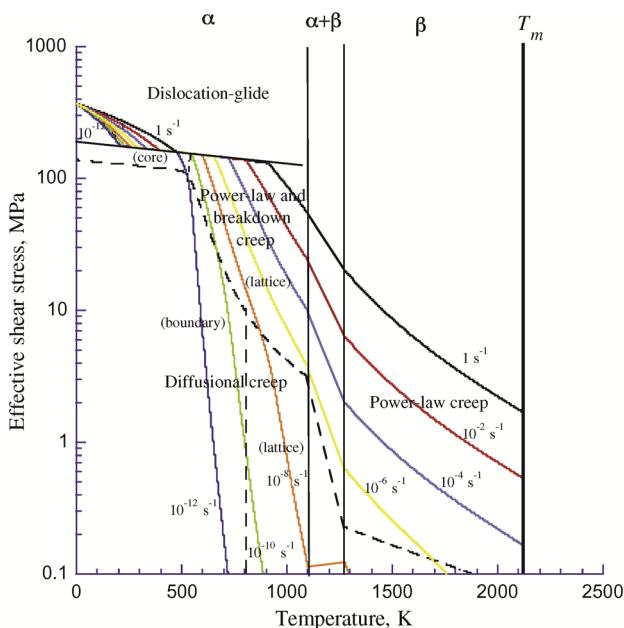


Fig. 2. A deformation-mechanism map for unirradiated zircaloy-4 with a grain size of  $150 \mu\text{m}$ . Reprinted from Wang et al.,<sup>5</sup> with permission from Elsevier.

stress state. This can be done within a finite-element calculation by incorporating mechanism-based models that include the appropriate activation energies, stress dependencies, and other material parameters. There is no need to make any a priori guesses about what creep law to include. Instead, the dominant law evolves naturally, and can change appropriately if the conditions change.

To develop such a model for zircaloy-4<sup>5</sup> the published thermal creep data for the alloy over the last 35 years were divided into groups of results from similar experimental conditions that each had remarkable internal consistency. These groups were

used to identify the creep mechanisms, based on the forms of the relationships between stress, temperature and strain rate, from which the appropriate activation energies and other associated creep parameters were deduced. Figure 2 shows the resultant deformation-mechanism map constructed for unirradiated zircaloy-4. It portrays how different creep mechanisms evolve and dominate under various stress and temperature conditions. By incorporating the concepts of such a creep-mechanism map into an FEM code, the controlling creep rate emerges naturally during any numerical analysis.

This framework and the implemented finite-element program provide an important tool for assessing the effects of stress and temperature in the early design stage, especially when multiple mechanism regimes are involved at the same time, or when the dominant mechanism changes over time. We have used it to simulate the creep-induced contact-force relaxation and structural deformation in the fuel assembly. Because the current deformation-mechanism map is for unirradiated zircaloy-4, additional models need to be developed to link the effects of radiation to creep, including irradiation growth.

## WEAR

Archard's relationship<sup>6</sup> is popularly used to describe the wear between two surfaces. The wear depth,  $w(s, t)$ , at any location along a contact,  $s$ , and time,  $t$ , can be calculated by integrating the governing equation:

$$\frac{\partial w}{\partial \Delta(s, t)} = \mu K p(s, t) \quad (1)$$

where  $K$  is the wear coefficient,  $p(s, t)$  is the local contact pressure,  $\Delta(s, t)$  is the local relative slip between the two surfaces at the contact, and  $\mu$  is the friction coefficient. The local wear rate,  $W = \partial w / \partial t$ , depends on the contact pressure, and even relatively small amounts of wear can change the profiles of the contacting bodies sufficiently to have a significant influence on the distribution of contact pressure.

The contact and wear problems are coupled, requiring an incremental algorithm for finite-element simulations. At each time step, the contact pressure is calculated based on the instantaneous morphology of the contact surfaces, and the local wear rate is obtained from the wear model. The morphology of the contact surface is then updated by adjusting the position of the surface nodes to match the wear. The process is then repeated for successive cycles. A well-known challenge with wear calculations is the need for constant remeshing to track the wear profile: it is not only computationally expensive but can also lead to numerical instability and non-convergence. We have developed an approach in which the morphology update is achieved by imposing fictitious eigenstrains in the elements at the contact surface. The magnitudes of these eigenstrains are calculated to produce the

change of surface morphology consistent with that caused by wear.<sup>7</sup> This method avoids severe numerical problems associated with remeshing, particularly if there are residual stresses induced by the slip process, and enables highly efficient modeling of wear evolution in GTRF that can be used with essentially all FEM packages.

## STRUCTURAL MECHANICS MODELING

### Multi-rod Grid Coupling

Traditional approaches<sup>8</sup> modeling turbulence-driven rod vibration adopt statistical characterizations of fluctuating fluid-pressure distributions on the rods, based on random vibration theory.<sup>9</sup> Each rod, modeled by elastic-beam theory, is coupled to grounded springs representing discrete points of mechanical interaction (contact, friction, sliding) with spacer-grid springs and dimples. Dynamic histories of point-contact force and relative sliding at each spring and dimple site are generated and analyzed for sliding wear work-rate. These histories can also be used to drive more detailed continuum modeling of the wear processes. Detailed continuum simulations incorporating structural creep and wear-scar evolution can be used to update grid/rod contact forces and/or gap openings, enabling simulations of continued turbulence-driven rod vibration.

We adopt certain features used in the VITRAN rod-vibration modeling software,<sup>10</sup> including the idealization of turbulent loading using a constant-amplitude, band-limited power spectral density (PSD) at discrete transverse point loads downstream of each spacer grid. The PSD magnitude scales that of observables such as mid-span velocity and acceleration, guiding calibration. An FFT algorithm spans the assumed frequency window, generating a set of temporal sine waves of random phase shift, constraining half of them to produce a real signal. Using explicit integration of projected modal dynamics, and accounting for solution-dependent grid/rod contact interactions, rod vibration is simulated over a sufficiently large time interval. Multiple realizations of random phase shifts provide converged estimates of the mean and the standard deviation of frictional work (rate) at each contact.

The support stiffnesses of the springs and dimples comprising a given grid cell facet's interaction with its adjacent fuel rod(s) are intrinsically coupled, owing to local bending flexibility of the orthogonal grid strips. Figure 3a shows a representative grid strip and illustrates the support coupling of two adjacent rods with the two dimples and one spring comprising a single panel of the grid cell. Non-negative contact forces  $F_I$  at the spring and dimples of a panel segment induce corresponding normal deflections  $\delta_J$ . A  $3 \times 3$  elastic stiffness matrix  $k_{IJ}$  connects these quantities according to  $F_I = k_{IJ}\delta_J$ .

Vibration simulations incorporating 2-sided coupled contact stiffness within structural mechanics models of multi-rod/multi-grid assemblies demonstrate spatial patterning of peak sliding wear work-rate. Figure 3b shows the spatial patterning of computed wear work-rate in a model  $5 \times 5$  assembly. Each rod was supported by 7 spacer grids and subjected to identical initial support conditions of zero gap and zero normal force, along with span-by-span turbulent loading of constant PSD. The peak mean wear work-rate at any contact point along each rod was normalized by that for a single rod identically supported by coupled grid panels comprising each spacer grid cell. No rod in the assembly had a peak wear work-rate exceeding that of the single-rod model, suggesting that the latter provides a conservative estimate. The peak wear work for the rod in the corner of the assembly that was supported externally by (stiff) dimples and internally by (compliant) springs matched that of the single rod, while that of the rod in the diagonally opposed assembly corner, supported externally by springs and internally by dimples, was only half as large, with intermediate values along external assembly edges having a dimple support. The reduced wear work-rates at interior rod locations are due to changes in average contact force because adjacent-cell rod contact elastically deflects contact points on shared grid cell panels. The spatial wearing patterns in this simple model bear similarities to patterns of leaking rods within a representative assembly, which are often concentrated along assembly external corners and edges.<sup>11</sup>

### Multi-rod Fluid-Structure Coupling

Typically, flow-induced vibrations in GTRF are modeled by studying the force spectrum on an isolated rigid rod interacting with an inflow at high Reynolds number. An important consideration is whether flow through a rod assembly causes geometric coupling with the fluid phase, resulting in certain rods receiving different forcing signatures than others.

This question can be addressed with a fluid-structure interaction study. The simulation method used is the Reference Map Technique,<sup>12,13</sup> an Eulerian numerical framework that permits the simulation of a dynamic fluid phase interacting with possibly nonlinear continuum solid phases on one numerical grid.

Five parallel rods are simulated, idealized as 2-D solid elastic bodies anchored firmly at their ends and weakly ( $10\times$  smaller) at three internal points to model grid supports. Anchoring is modeled with spring forces spread over the pictured interaction area (Fig. 3c). An incoming transverse fluid flow is introduced. To bring out possible coupling of rod motions, the rods are given an artificially high



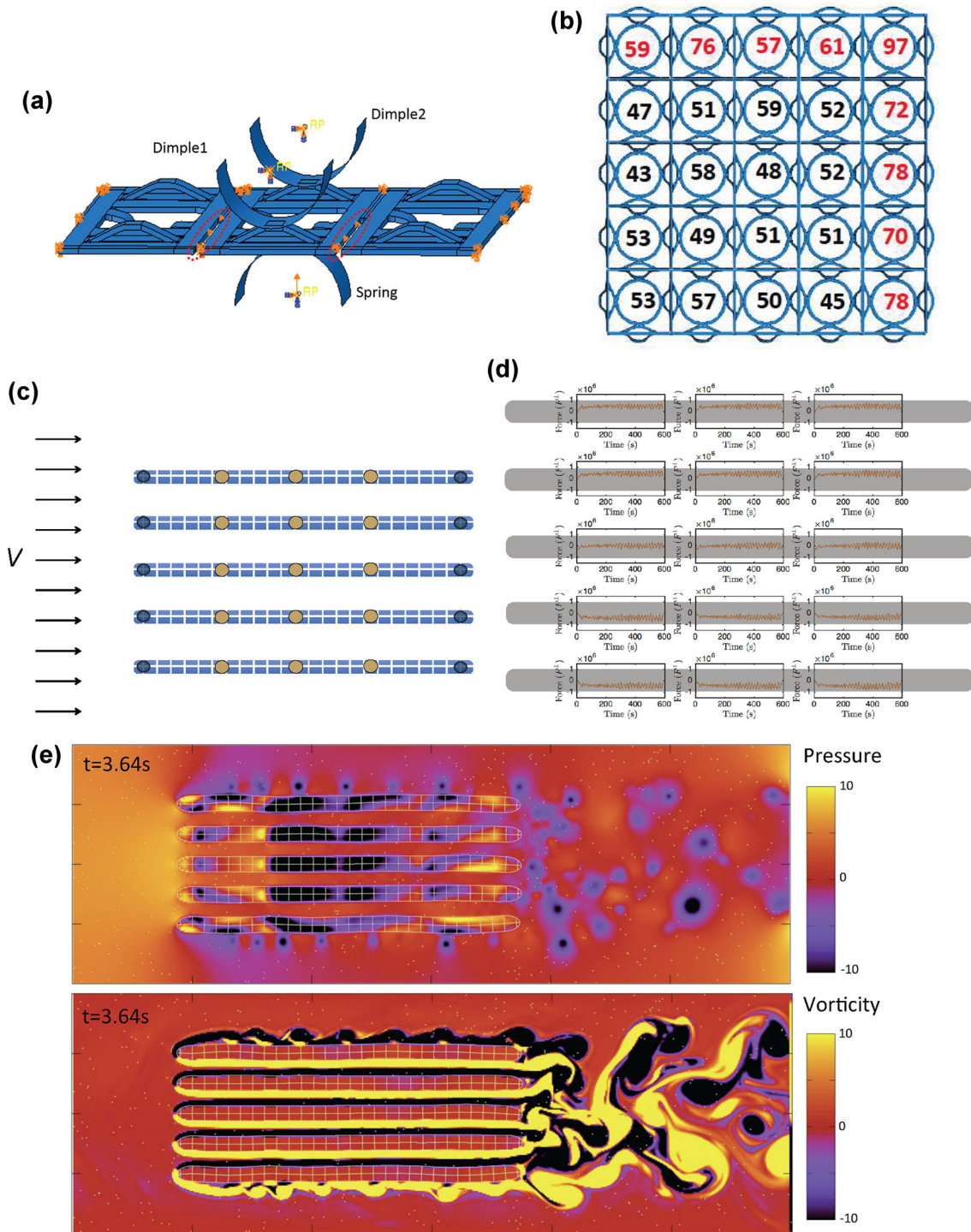


Fig. 3. (a) Schematic illustration of rod contacts at the 2 dimples and 1 opposing spring comprising a panel of a spacer grid cell. Contact force at any site on the panel elastically deflects all grid contact points on the panel segment. (b) Summary of normalized mean peak wear work-rate, in per cent, for a model 5 × 5 rod assembly. Normalization is with respect to the corresponding mean peak work in a single-rod model, supported at each spacer grid by four stiffness-coupled panels. (c)–(e) include fluid. (c) Simulation setup of five rods anchored at their ends subject to a rightward incoming uniform flow. Weak supports provided at three interior locations. (d) Transverse forces at the interior supports on each rod. (e) Snapshot of relative pressure and vorticity (in SI) during simulation.

elastic compliance. Non-laminar fluid motion generates flow-induced vibrations of the rods (Reynolds number = 12,000; see Fig. 3e).

A fluctuating force of the grids on the rods is apparent, consistent with turbulent flow induced vibration of the rods. Interestingly, there is also a

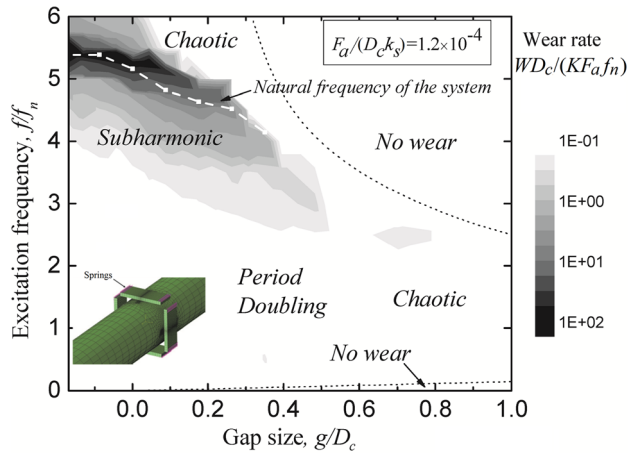


Fig. 4. A wear-rate map for a large spectrum of gap sizes and excitation frequencies. The excitation frequency is  $f$ . The first natural frequency for the vibration of a free rod is  $f_n$ . The inset shows the 3-D model: a fuel rod with a cladding thickness of  $D_c$ , four support plates each connected to springs with a stiffness of  $k_s$ , and the gap between the rod and the plate is  $g$ . The amplitude of force exerted on the rod by the turbulent flow is  $F_a$ . The critical gap size, which is associated with the maximum wear rate, lies within the subharmonic regime. In the no-wear region, the amplitude of the rod vibration is smaller than the gap size so that no impact between the rod and plate can happen. The curve of the natural frequency of the system appears to overlap with the peaks in the contour.<sup>14</sup>

non-negligible mean normal force, which vanishes on the central rod and pushes outward on the extreme rods (Fig. 3d). A mean force is rarely if ever considered in typical FIV studies used as inputs to GTRF. As previously noted, rods at the extremal locations of an assembly tend to be more susceptible to wear.<sup>11</sup> Likewise, fluid coupling of the rod system appears to provide another explanation for this effect, on top of the effect of grid-wise coupling described previously.

### EFFECTS OF GAP SIZE AND EXCITATION FREQUENCY ON GTRF WEAR

The wear rate is sensitive to the gap size between the rod and grid. A close fit between them results in a larger contact pressure and frictional force, leading to a higher wear rate if sliding happens. A tight fit can make it difficult for sliding to happen, leading to a lower wear rate. Conversely, a loose fit may result in dynamic impacts during oscillation, leading to a higher wear rate. However, if the gap size is too large, the amplitude of oscillation may be insufficient to cause regular contact, leading to a very low wear rate. Obviously, this would not be desirable, despite the low wear rate, because the grid would not sufficiently support the fuel rod.

The wear rate also depends on the excitation frequency from the coolant flow. The frequency and amplitude of the responding vibration of the rod are intercorrelated. As we show here, even if one assumes a periodic excitation frequency from the flow, the rod responds in a complicated fashion,

exhibiting subharmonic, period-doubling and chaotic modes of vibration, depending on the excitation frequency and gap size.

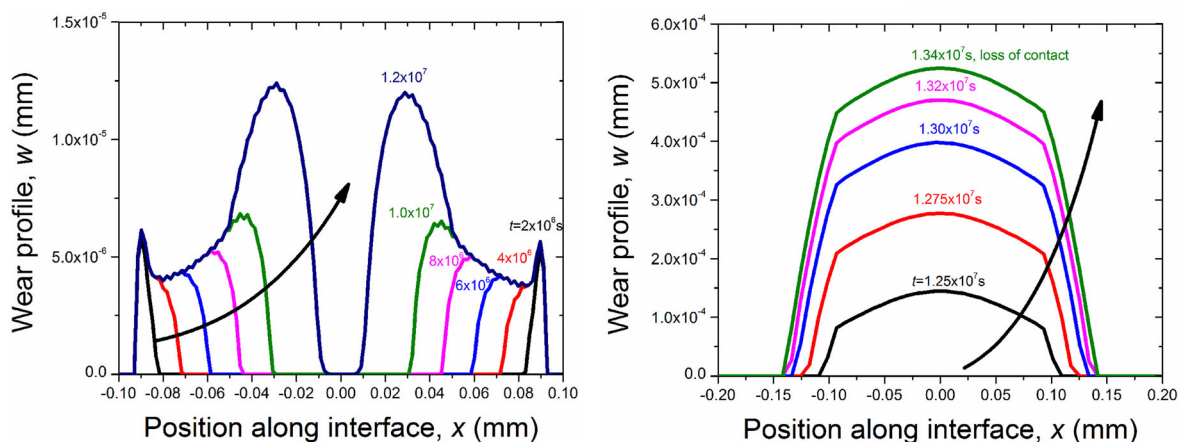
We have developed 3-D finite-element modeling to investigate (1) the dynamic response of a fuel rod under the driving forces of various frequencies induced by the coolant, (2) the effects of the gap size and initial interference on the wear rate of the rod, and (3) the effect of the excitation frequency on the wear rate. Figure 4 shows the dependence of the wear rate on the gap size and excitation frequency.<sup>14</sup> There is a critical size of gap that corresponds to a subharmonic response, and which causes a maximum rate of wear for a given excitation frequency. The gap size that results in a maximum wear rate for a given excitation frequency corresponds to the gap size that results in the excitation frequency matching the natural frequency of the system, where the natural frequency is defined as being the frequency of the first mode of free vibration of the system consisting of the rod and support plates. This finding suggests that the maximum wear rate is directly related to the natural resonance of the system. When the gap is larger than the critical size for a given excitation frequency, the response of the rod becomes chaotic, and the wear rate reduces greatly.

### COUPLING WEAR AND CREEP

The characteristic time scales of creep and fretting wear are quite different. A single cycle of wear can occur within a second. In contrast, significant creep can take place at the scale of days or months. Using the small time increments suitable for modeling each wear cycle would be too computationally expensive and impractical. On the other hand, using the relatively large time increments suitable for creep may miss significant changes in contact stress induced by wear.

To resolve this large difference in time scales, we have developed an “effective-cycle” approach. Up to some limit, several successive vibration cycles can be combined into a single effective cycle with a larger period without loss of accuracy. In calculating an optimal effective period, it is noted that both wear and creep cause stress redistribution, and both affect each other because of this stress change. The effective-cycle technique takes care of this interaction systematically. For instance, creep causes stress relaxation within each effective cycle, and this change in stress inherently interacts with the wear calculation, since both wear and creep are calculated simultaneously at each time step within the effective cycle. The period of the effective cycle is adjusted dynamically based on the current rate of stress relaxation from both creep and wear in accordance with any required accuracy. This automatic adjustment is achieved by continuously monitoring the change of contact pressure.

### Wear profile evolution (arrow shows increasing time)



### Contact force relaxation

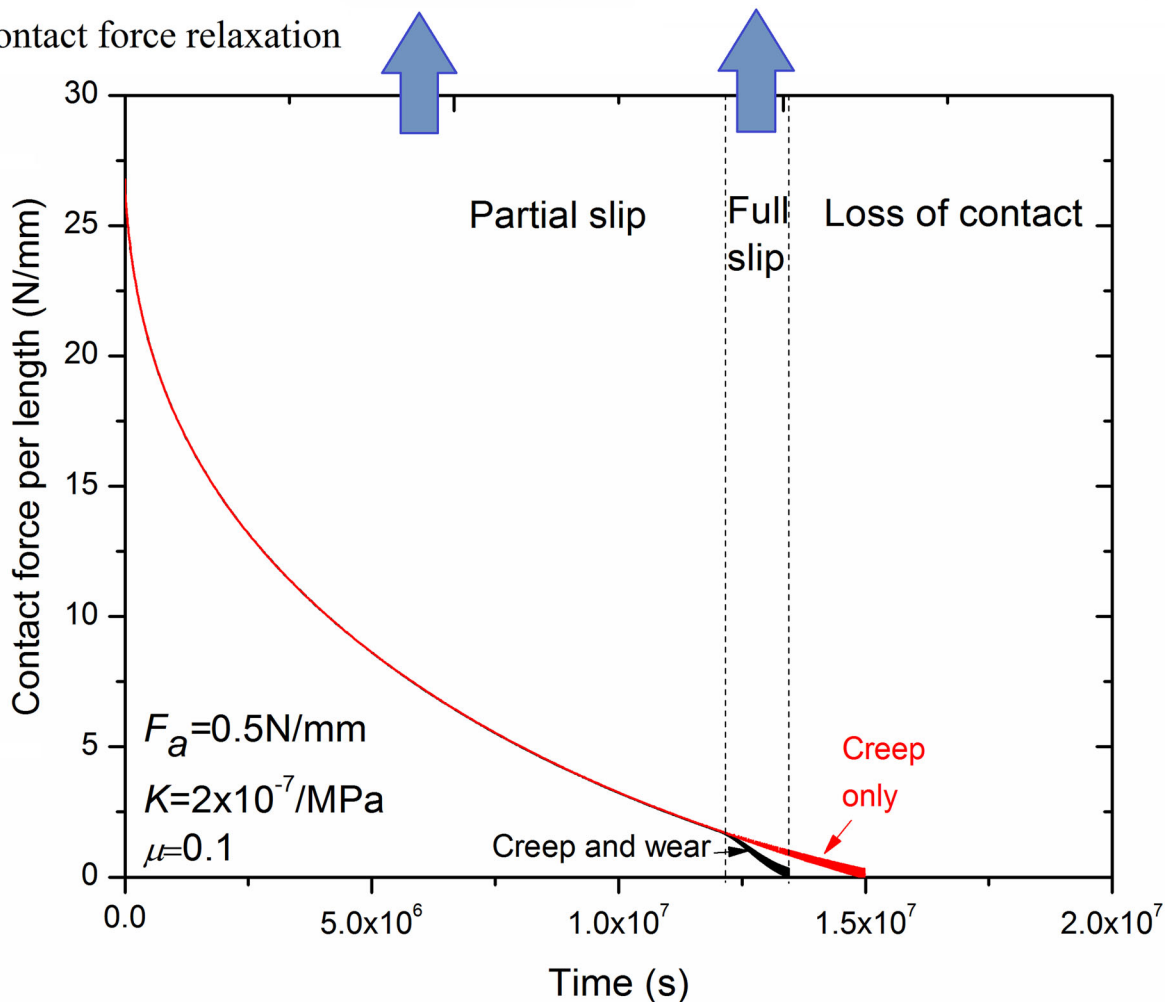


Fig. 5. The contact force, or integrated normal pressure over the contact surface, relaxes over time. The amplitude of force per rod length exerted on the rod by the turbulent flow is  $F_a$  with a period of 0.1 s. Two stages exist: partial slip and full slip. When partial slip occurs, creep dominates the stress relaxation. When full slip occurs, wear becomes the dominant stress relaxation mechanism. The wear scar shows different geometry in the partial slip and full slip stages.<sup>15</sup>

The effective-cycle approach, the fictitious eigen-strain approach for wear, and the mechanism-based creep model have been coupled to evaluate gap

formation in GTRF. These three tools were used to model gap formation in a 2-D model of a unit thickness in the axial direction of the rod. Figure 5



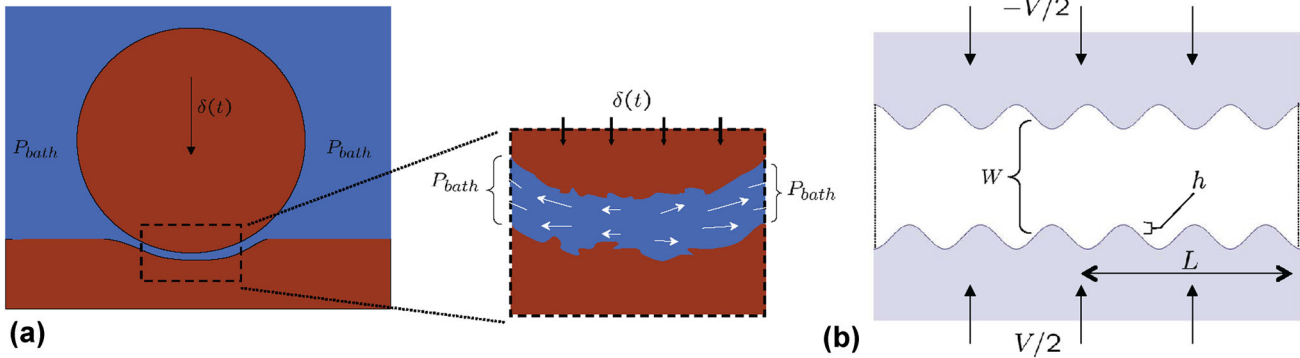


Fig. 6. (a) Not-to-scale illustration of roughened rod and dimple surfaces making contact in a fluid. (b) Simplified lubrication model.

shows the contact force relaxation process.<sup>15</sup> For comparison, stress relaxation if only creep is active, and no wear, is shown on the figure. The comparison shows that when partial slip occurs, creep dominates the stress relaxation. When full slip occurs, wear becomes the dominant stress relaxation mechanism. The result not only gives a prediction of the service time before loss of contact but also shows that the process comprises two stages: partial slip where wear happens at the edge of the contact surface, and full slip where wear happens at the entire surface. Though the amount of wear is smaller in the partial slip stage, this stage occupies most of the time and therefore partial slip is important in GTRF. The wear scar shows different geometries in the two stages.

At present we have not coupled the chaotic effects of turbulent flow, and the excitation force was modeled as a sinusoidal wave. In future studies, the excitation force will be replaced by the full spectrum obtained from computational fluid dynamics.

### INFLUENCE OF FLUID IN OPEN GRID-ROD GAPS

One potential factor yet to be discussed is the role the coolant fluid plays in the wearing process. In early stages when gaps remain closed or separated only marginally, there is evidence the presence of stationary fluid does not significantly change rates of wear;<sup>16</sup> however, when fluid is flowing over the contact region, wear rates can increase notably due to particles being carried off by the flow. As gaps open further, the effect of the fluid can become more severe, as separated surfaces produce a squeeze-film of fluid that assists in removing third-body particles and builds up hydrodynamic stresses as contacts form. It has been shown that wear rates increase directly with gap size beyond a critical gap opening in fluid submerged tests.<sup>17</sup> Among various wearing conditions, it was shown<sup>18</sup> that grid-rod interactions in a fluid with separation sufficient to permit impacts produce an effective wear coefficient  $\sim 100$  times larger than that of dry rods in close sliding conditions.

The effect of fluid can be understood considering a simplified version of the system. Figure 6 shows a model system of a submerged roughened rod making contact with a roughened dimple surface, bounded by a bath pressure.

In the limit of a roughness-free surface, as the gap closes fluid strain-rates grow to hypothetically unbounded values. This can aid in particle removal processes discussed previously, and, notably, cause a hydrodynamic stress blow-up. In the rough case, these stresses can assist wearing and lubrication analysis<sup>19</sup> reveals peak pressure in the center of the roughened gap region, exceeding the bath pressure by  $\sim 6\eta VL^2(W^2 + h^2)/W^5$  and the fluid shear stress along the surfaces grows from the center out, reaching a peak value of  $\sim 1.5\eta VL/(W/2 - h)^2$ , where  $\eta$  is the viscosity. The substantial rate these stresses grow as gaps close (i.e.  $W/2$  approaches  $h$ ) suggests fluid stress on surfaces can contribute in the surface removal process.

To study this effect more completely, a two-way submodeling capability is being built into the fluid-solid interaction method from the “[Structural Mechanics Modeling](#)” section to permit coupled simulation of the rod-scale turbulent fluid motion, and the contact-scale lubrication behavior. The routine models the system with two separate numerical domains: a fine-grid region encompassing the fluid-solid contact zones, and a coarse-grid domain for the remainder of the problem. The two domains are coupled through their mutual boundary using interpolation. The key benefit is the smaller time-step of the refined domain does not limit the time-step of the larger, coarse domain. Initial verifications of the submodeling approach were applied to a nonuniformly deforming solid with a localized stress-concentration region. When the stress-concentrated zone was refined two times using submodeling, the simulated motion on the whole gives the same  $L_2$  accuracy as a simulation with a uniform refined grid, but the submodeled simulation completes 5 times faster. This ability to multi-scale the numerics will be key to simulating the widely separated scales of fluid-solid interaction occurring in GTRF within a reasonable time.

## CONCLUSION

The wear caused by GTRF is a complex and challenging problem, which is significant to the operation of PWRs. Solving the GTRF-related problems requires integrating a number of different areas, including structural mechanics, deformation mechanisms under high-temperature and irradiation conditions such as creep and irradiation growth, fretting wear, computational fluid dynamics, and vibration. Some of the integration, such as of vibration, creep and wear, has been performed. More work needs to be done to integrate other areas, such as turbulent excitation forces from fluid dynamic simulations, and processes such as corrosion on the surface of the fuel rod, which can alter the friction coefficient and wear coefficient.<sup>20</sup> Experimental validation is an on-going challenge for GTRF models. An ideal GTRF wear tester would operate under conditions that simulate the fuel-rod contact stresses, motions, coolant flow, frequency, amplitude, temperature, and state of irradiation. CASL is currently designing a unique GTRF simulative wear bench tester: autoclave fretting-impact wear (AFIW) tester. This new equipment is designed to handle actual cladding and grid samples in heated pressurized water at temperatures up to 220°C and pressures up to 2.4 MPa. Once the tester is available, systematic wear tests will be conducted at CASL at the modes of fretting only, impact only, and fretting plus impact. The creep and wear calculation developed at the University of Michigan, and the power spectrum analysis of the turbulent excitation forces developed at the Massachusetts Institute of Technology will be integrated. This paper highlights some completed and on-going research related to the GTRF problem, which we hope to provide an understanding of the current status and to stimulate the interest to continue exploring GTRF-related problems.

## ACKNOWLEDGEMENTS

This research was supported by the Consortium for Advanced Simulation of Light Water Reactors (<http://www.casl.gov>), an Energy Innovation Hub (<http://www.energy.gov/hubs>) for Modeling and Simulation of Nuclear Reactors under US Department of Energy Contract No. DE-AC05-00OR22725.

## REFERENCES

1. K. Edsinger, J. Deshon, A. Kucuk, E. Mader, B. Cheng, S. Yagnik, and R. Daum, Recent US fuel reliability experience. in *Proceedings of the Water Reactor Fuel Performance Meeting—WRFPM/Top Fuel 2009* (2009).
2. K.T. Kim and J.M. Suh, *J. Nucl. Sci. Technol.* 46, 149 (2009).
3. Y.H. Lee and H.K. Kim, *Wear* 301, 569 (2013).
4. K.T. Kim, *J. Nucl. Mater.* 433, 364 (2013).
5. H. Wang, Z. Hu, W. Lu, and M.D. Thouless, *J. Nucl. Mater.* 433, 188 (2013).
6. J.F. Archard, *J. Appl. Phys.* 24, 981 (1953).
7. Z. Hu, W. Lu, M.D. Thouless, and J.R. Barber, *Tribol. Int.* 82, 191 (2015).
8. P.R. Rubiolo, *Nucl. Eng. Des.* 236, 1628 (2006).
9. P.H. Wirsching, T.L. Paez, and K. Ortiz, *Random Vibrations: Theory and Practice* (New York: Wiley, 1995).
10. P.R. Rubiolo and M.Y. Young, *J. Power Energy Syst.* 2, 57 (2008).
11. Z.E. Karoutas, M.A. Krammen, Y. Aleshin, R.L. Kesterson, and S.F. Grill, Prediction of grid to rod gap for fuel rod vibration analysis in PWR cores. in *Proceedings of the Water Reactor Fuel Performance Meeting—WRFPM/Top Fuel 2009* (2009).
12. K. Kamrin, C.H. Rycroft, and J.C. Nave, *J. Mech. Phys. Solids* 60, 1952 (2012).
13. B. Valkov, C.H. Rycroft, and K. Kamrin, *J. Appl. Mech. Trans. ASME* 82, 041011 (2015).
14. Z. Hu, M.D. Thouless, and W. Lu, *Nucl. Eng. Des.* (in press) (2016).
15. H. Wang, Z. Hu, W. Lu, and M.D. Thouless, *Nucl. Eng. Des.* (submitted) (2016).
16. J.S. Kim, S.M. Park, and Y.Z. Lee, *Tribol. Trans.* 53, 452 (2010).
17. K.T. Kim, *Nucl. Eng. Des.* 239, 2820 (2009).
18. H.K. Kim and Y.H. Lee, *Wear* 263, 532 (2007).
19. B.J. Hamrock, S.R. Schmid, and B.O. Jacobson, *Fundamentals of Fluid Film Lubrication* (Boca Raton: CRC Press, 2004).
20. P.J. Blau, *Wear* 313, 89 (2014).